

Tomographic search for missing link between the ancient Farallon subduction and the present Cocos subduction

Alexei Gorbatov and Yoshio Fukao

Institute for Research on Earth Evolution, JAMSTEC, 2-15 Natsushima-cho, Yokosuka, Japan. E-mail: alexei@jamstec.go.jp

Accepted 2004 October 15. Received 2004 October 14; in original form 2003 November 13

SUMMARY

A striking feature of the tomographic images of the Earth's mid-mantle is the long, high-velocity belt extending in a north–south direction under the North and South American continents, which is believed to be the remnant subduction of the Farallon Plate. In the Oligocene epoch the North Farallon Plate subduction terminated off Baja California and the South Farallon Plate broke into the Cocos and Nazca plates. This important period of the Farallon subduction history is not clearly understood, due in part to the lack of high-resolution tomographic images. Our *P*-wave tomographic image of the mantle below Mexico indicates that the currently subducting slab of the Cocos Plate is torn apart from the already subducted slab of the ancient Farallon Plate in a region behind the slab window or slab gap off Baja California. We suggest that the southeastward advance of this slab tearing was synchronous with the counter-clockwise rotation of the Cocos Plate against the eastward to northeastward subduction of the ancient Farallon Plate. The Cocos slab torn apart from the deeper Farallon slab dips to the north to northeast with its strike oblique to the trench axis. This slab configuration delineates well with the intermediate-depth earthquake activity and the volcanic activity known as the Trans Mexican Volcanic Belt. Further to the south of the slab tearing of the subducted slab continues from the deeper Farallon part to the shallower Cocos part but with considerable distortion in the shallower part.

Key words: Cocos Plate, Farallon Plate, seismicity, tomography, volcanic activity.

1 INTRODUCTION

Upon the approach of the East Pacific Rise to the Americas, the Farallon Plate broke up into the North and South Farallon plates in the Eocene. This event was followed by the creation and subsequent widening of a slab window (Dickinson & Snyder 1979; Thorkelson 1996) or a slab gap (Severinghaus & Atwater 1990) off Baja California. The remnant of the Farallon slab in this region has been tomographically imaged by van der Lee & Nolet (1997). The South Farallon Plate was fragmented into the Cocos and Nazca plates at about 25 Ma (Severinghaus & Atwater 1990; Barckhausen *et al.* 2001). The subducted slab of the Nazca Plate has been tomographically imaged as a subhorizontally flattened slab either above the 660 km discontinuity (as in Chile) or below it (as in Peru) (e.g. Fukao *et al.* 2001). The tomographic image of the North Farallon slab extends through the mid-mantle down to a depth of ~1500 km (e.g. Grand *et al.* 1997; van der Hilst *et al.* 1997). Its upward extension is truncated in the mantle transition zone without continuing up to the surface and its southern end has been located near the border of the USA and Mexico at ~30°N (van der Lee & Nolet 1997).

No published tomographic study has yet described how the North Farallon slab meets the South Farallon slab and how the latter continues to or discontinues from the shallower Cocos Plate. Our aim

is to make a tomographic search for this missing link between the North and South Farallon slabs and the Cocos slab.

2 DATA AND METHOD

We used an extensive global catalogue of *P*-wave traveltimes recompiled by Engdahl *et al.* (1998) with successive updates, including the recent Mexican regional network data, to infer the compressional wave velocity structure below Mexico. The hypocentral parameters were fixed throughout the inversion to those in the updated catalogue of Engdahl *et al.* (1998) due to the inclusion of depth phases (*pP*, *pwP*) used for their determination. The study area was parametrized by 19 layers and blocks with sides of 50 × 50 km in the uppermost mantle, gradually increasing in size to 2° × 2° in the middle mantle at a depth of 1500 km. The whole Earth's mantle outside the target region was parametrized by 16 layers and blocks with sides of 5° × 5° to complete a global model construction. Although only the regional model is of interest to us, velocity anomalies of all the blocks relative to the reference earth model AK135 (Kennett *et al.* 1995) were determined simultaneously to avoid spurious mapping of the surrounding structures into the regional image. A 3-D seismic ray tracing algorithm (Koketsu & Sekine 1998) was used to determine each ray path between the source and receiver. Our set of

linear equations consists of more than 81 000 blocks and 1 631 000 ray paths. Several successive iterations with the updates of mantle structure and ray-path trajectory were performed using the LSQR solver. The misfit between the observed seismic data and the reconstructed earth model was measured in terms of the root mean square (RMS) of residual traveltimes. The RMS value was 1.95 s before the iteration, which decreased to 1.37 s after the third iteration with a subsequent RMS change of less than 0.01 s. We terminated the inversion at the fourth iteration. We performed a series of tests to ensure the robustness of our results. The tests include the synthetic structure resolution test and the checkerboard resolution test. The synthetic test showed that the input slab structure can be reconstructed all along its extension but with low-amplitude vertical smearing in some parts of the upper mantle. The checkerboard test indicated that alternate patterns in scales similar to those of subducted slabs can be recovered, but with variably reduced amplitudes and with smearing, especially near the border of our regional model, as will be discussed further.

3 RESULT

Fig. 1 shows the tectonic map of the study area, where five lithospheric plates are involved (Pardo & Suarez 1995; Lonsdale 1991; Nicholson *et al.* 1994). As the curved traces of the fracture zones on the seafloor indicate, the Cocos Plate subducts at a rate that rapidly decreases northwest from 7.5 cm yr⁻¹ at 94°W to 4.8 cm yr⁻¹ at 104.5°W (DeMets *et al.* 1990). The Wadati–Benioff zone is confined in the uppermost mantle. Its leading edge is east–west trending to the west of ~96°W. Notably this trend is parallel to the Trans Mexican Volcanic Belt but is oblique to the Middle American Trench. On the other hand, the Wadati–Benioff zone to the east of ~96°W is almost parallel to the trench (Pardo & Suarez 1995). Fig. 1 also locates the three northeast–southwest profiles and one east–west profile, which will be referred to in Figs 2 and 3.

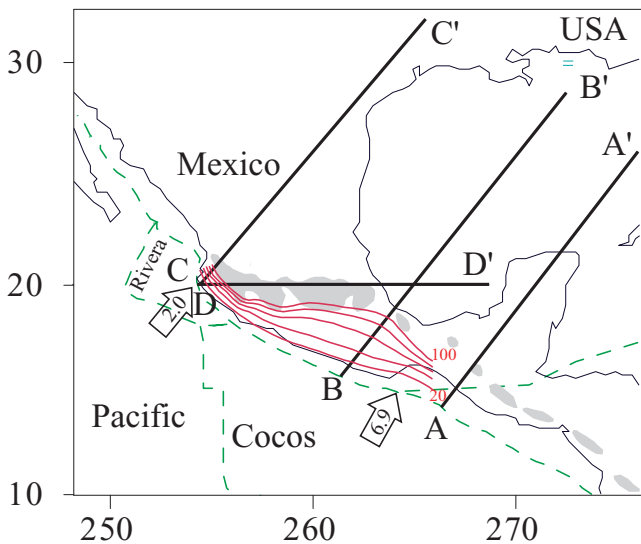


Figure 1. Tectonic framework of the study area. The dashed curve shows the boundaries between tectonic plates. The Trans Mexican Volcanic Belt is shown as a grey shaded zone. Red curves are isodepth contours of the Wadati–Benioff zone with a 20 km interval (after Pardo & Suarez 1995). Arrows with numbers inside indicate the direction and rate in cm yr⁻¹ of plate subduction below the Americas. Profiles AA' to DD' will appear in Figs 2 and 3.

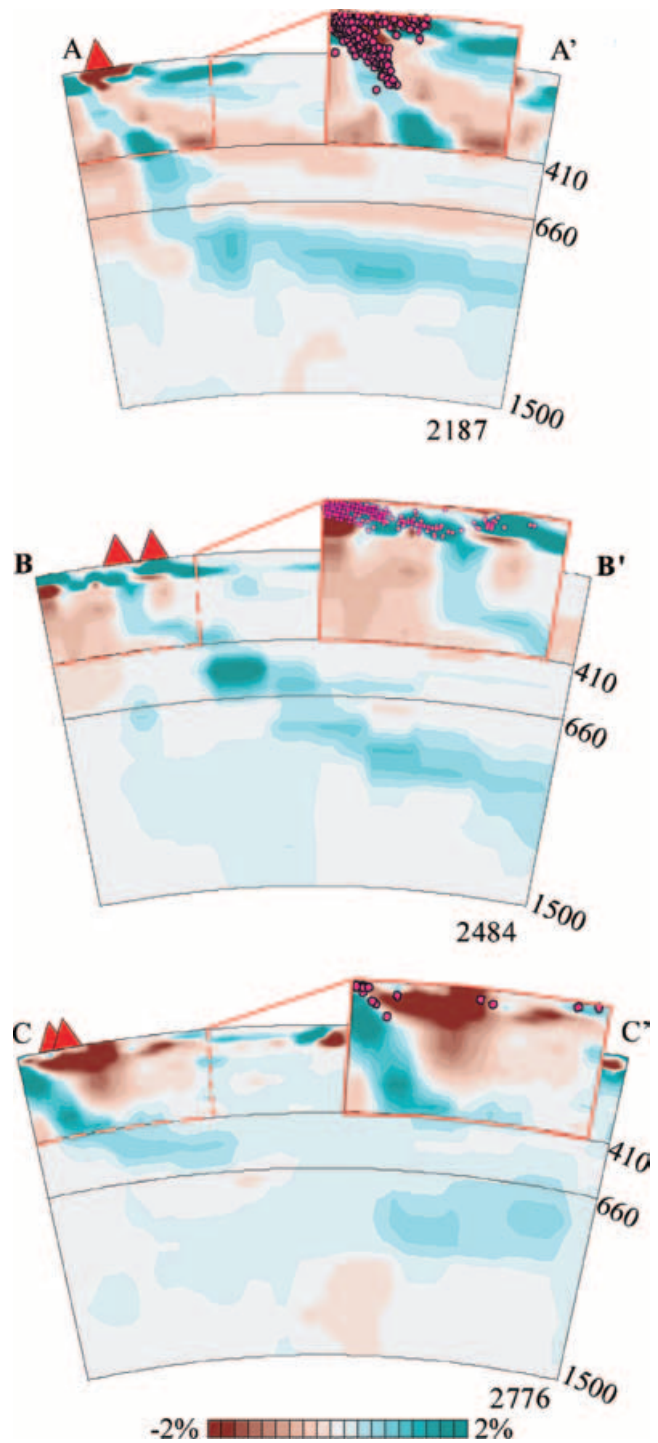


Figure 2. Cross-sections of the *P*-wave tomographic model along profiles AA' to CC' whose locations are given in Fig. 1. Positive and negative velocity anomalies (in per cent) relative to the reference earth model AK135 (Kennett *et al.* 1995) are indicated in blue and brown, respectively. Red triangles are volcanoes. The left upper corner of each cross-section is the zone of plate insertion, which is highlighted by a red dashed line with its enlarged image in the inset where the earthquake hypocentres are indicated in purple.

Fig. 2 shows the tomographic cross-sections along the northeast–southwest profiles. Each of the insets is a zoomed-in view of the shallower part of the subduction zone with a projected earthquake hypocentral distribution. The subducted slab image in the uppermost

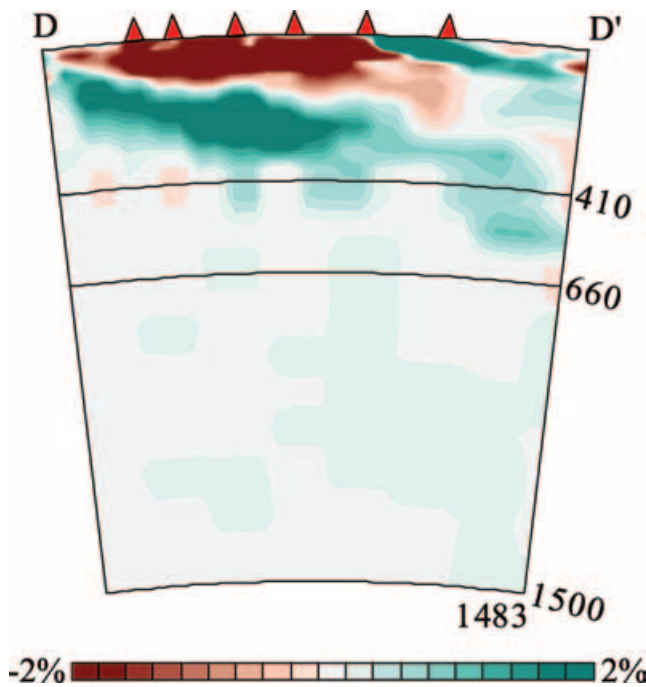


Figure 3. Cross-section along profile DD' almost parallel to the Trans Mexican Volcanic Belt (see Fig. 1). The legend and all symbols are the same as those in Fig. 2.

mantle is subparallel to the uniquely configured Wadati–Benioff zone. For example, the imaged slab is dipping steeply along profile AA' but is almost horizontal along BB', and this rapid change well mimics the lateral change in configuration of the Wadati–Benioff zone. Along either profile AA' or BB' the slab extends to depths beyond the leading edge of the Wadati–Benioff zone in a complex way to cross the 660 km discontinuity, below which it lies subhorizontally or dips gently in the mid-mantle. Along profile CC', on the other hand, the slab flattens above the 660 km discontinuity and is apparently detached with a large gap from the deeper part that lies well below the 660 km discontinuity.

Fig. 3 shows the cross-section along the east–west profile DD' subparallel to the Trans Mexican Volcanic Belt (Pardo & Suarez 1995; Ferrari *et al.* 1999), where the slab subducted from the trench dips very gently to reach a depth of ~200 km, above which the mantle is extensively slow. This anomalously slow uppermost mantle just above the almost flat slab is a unique feature under the Trans Mexican Volcanic Belt: no such extensively slow anomaly develops above the slab further to the south where the slab runs parallel to the trench. Fig. 4 shows the result of a checkerboard resolution test along profile DD', demonstrating that the upper mantle features are resolved well by our tomography.

4 SLAB TEARING

Fig. 5 shows the Cocos–Farallon slab system revealed by the seismic tomography. This slab system was used to trace the upper surface of the high-velocity slab by isodepth contours presented in Fig. 6. In this contour map, our detailed study is limited to the west of 95°W. The contours further east in the depth range ~900–1500 km were drawn using the tomographic model of Gorbатов *et al.* (2001); the use of other models (e.g. Grand *et al.* 1997; van der Hilst *et al.* 1997) would not give significant differences for contouring. The subducted slab in this depth range represents the remnant of the Farallon slab in

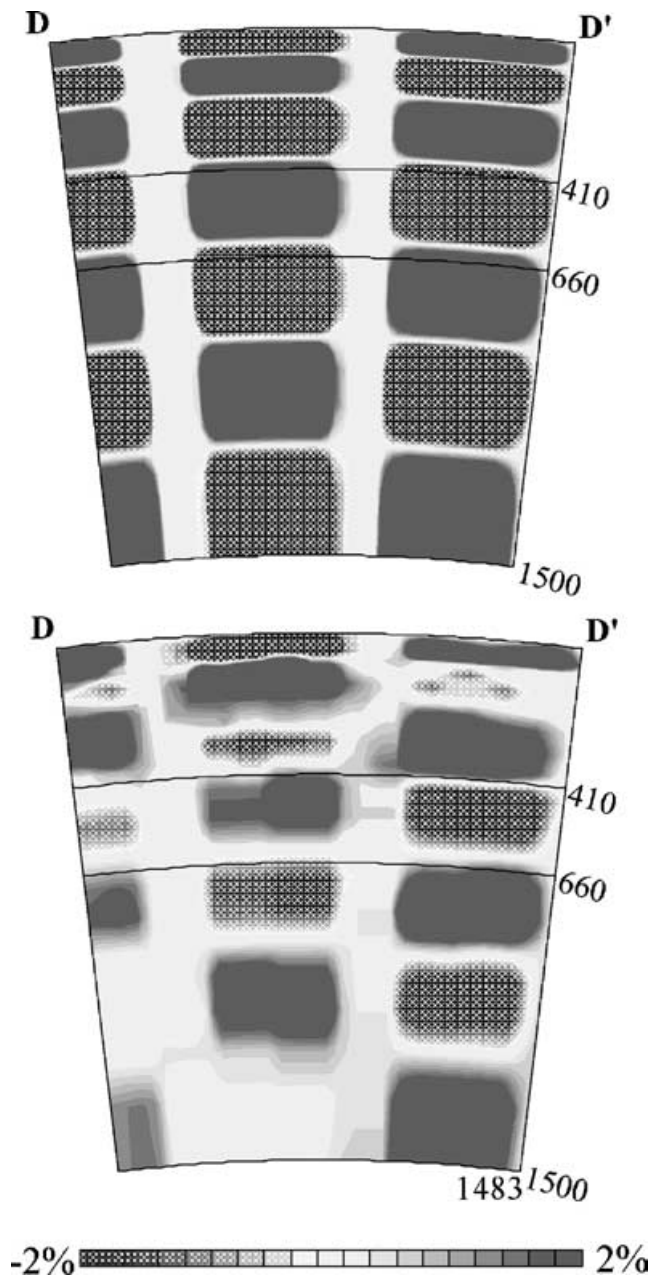


Figure 4. Synthetic resolution test of the tomographic model along cross-section DD'. The upper image shows the initial synthetic model while the lower one is the recovery of the initial synthetic model contaminated with random noise.

the Late Mesozoic–Early Cenozoic where the convergence boundary was oriented subparallel to the west coast of North America, which migrated progressively westwards (Engebretson *et al.* 1985; Stock & Molnar 1988).

In the uppermost mantle the contours of the Cocos slab almost coincide with those of the Wadati–Benioff zone so that only the latter is shown in red in Fig. 6 by referring to Pardo & Suarez (1995). The Trans Mexican Volcanic Belt is bounded geographically by the 100 km and 200 km isodepth contours of the subducted slab. To the south of ~20°N the shallower slab of the Cocos Plate is apparently continuous to and indistinguishable from the deeper slab of the Farallon Plate (cross-sections AA' and BB' in Fig. 2). On the other hand, to the north of ~25°N the Cocos slab, including the subducted part

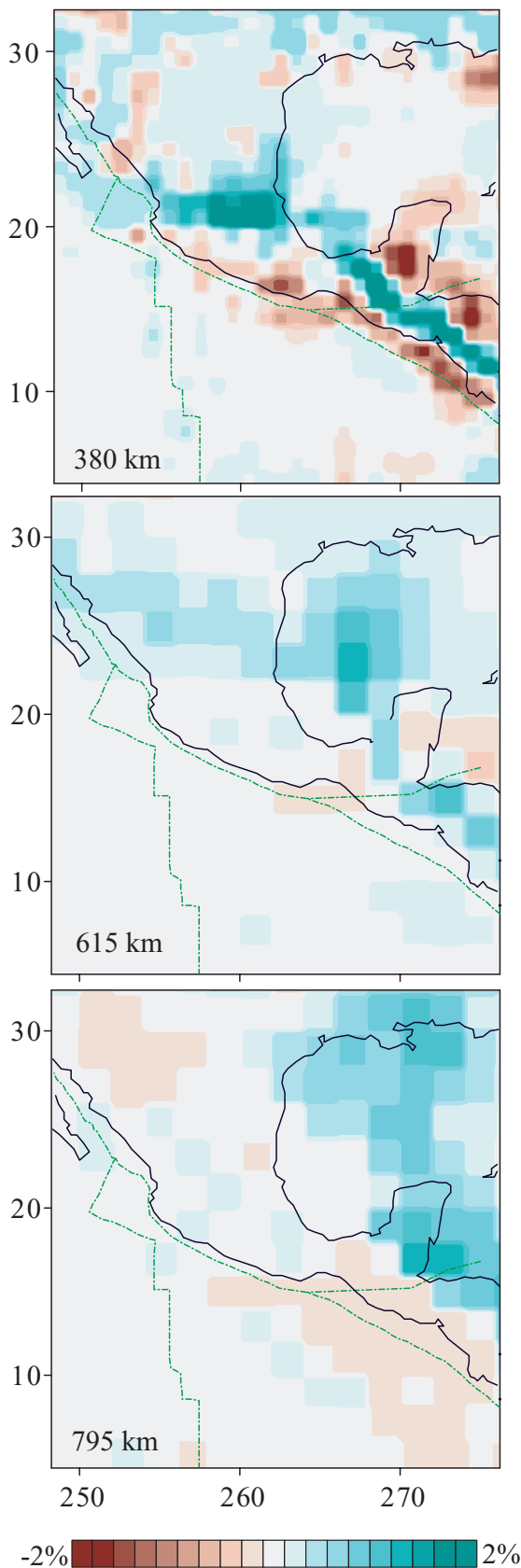


Figure 5. Three selected slices from the tomographic image of Mexico. Depth is indicated at the left lower corner of each slice. A velocity anomaly scale (in per cent) relative to the reference earth model AK135 (Kennett *et al.* 1995) is shown at the bottom.

of the Rivera Microplate, is detached from the Farallon slab, and the gap widens northwards (profile CC' in Fig. 2). This detachment is most likely due to slab tearing, which is geometrically required because of the mismatch in the subduction rate between the Cocos and Farallon plates. The rate of the present day Cocos subduction decreases rapidly northwestwards, while the rate of the Farallon subduction before ~ 25 Ma was almost uniform along the hypothetical trench line in the relevant region (e.g. Engebretson *et al.* 1985; Stock & Molnar 1988; Lithgow-Bertelloni & Richards 1998).

5 DISCUSSION

Fig. 7 schematically illustrates the successive sequence of plate subduction during the past 40 Myr. Fig. 7(a) (40 Ma) represents the stage shortly after the break-up of the Farallon Plate into the northern and southern Farallon plates. The diffuse boundary between the two plates (Severinghaus & Atwater 1990) was located near the upper frame of the diagram. At about 25 Ma (Fig. 7b) the ridge-transform fault system intersected the trench off northwest Mexico to create the slab window (Dickinson & Snyder 1979; Thorkelson 1996) or slab gap (Severinghaus & Atwater 1990). The Farallon slab, below the slab window, was detached from the surface plate so that it lost resistance against its descent. The Farallon slab to the south of the slab window, on the other hand, remained continuous to the young surface plate which was resistive against subduction. Because of this contrast the subducted part adjacent to the slab window began to be torn apart to separate the deeper part (Farallon slab) from the shallower part (Cocos slab). It was at about the same time that the Cocos–Nazca spreading centre began to open (Barckhausen *et al.* 2001) by a mechanism such as that suggested by Wortel & Cloetingh (1981), resulting in the break-up of the South Farallon Plate into the Cocos and Nazca plates. The counter-clockwise rotation of the Cocos Plate was due primarily to the resistance against subduction near its northwest end. Figs 7(c) and (d) illustrate the subsequent stages up to the present. The slab tearing progressively advanced southeastwards, and accordingly the gap between the deeper part (Farallon slab) and the shallower part (Cocos slab) progressively widened. The Cocos slab, torn apart from the Farallon slab, dips northwards to northeastwards, leading to the eastward to southeastward trending volcanic belt (Fig. 4; Ferrari *et al.* 1999). Detachment of the Farallon slab from present-day subduction was suggested in earlier tomographic studies (e.g. van der Hilst 1990). However, further to the southeast the slab has remained continuous from its shallower to deeper parts, where the counter-clockwise rotation of the shallower part (Cocos slab) versus the eastward to northeastward subduction of the deeper part (Farallon slab) caused a complex slab distortion, as seen along profiles AA' and BB' in Fig. 2. The almost flat configuration of the subducted slab in the uppermost mantle along profile BB' might have been responsible for the uplift and tectonic erosion of the southwestern continental margin of Mexico in the 35–25 Ma age range as inferred by Moran-Zenteno *et al.* (1996).

Fig. 8 schematically explains the geometric effect of slab tearing by using a paper sheet which is intended to be a miniature of the slab. In this illustration the miniature slab is torn apart into the Farallon part to the east and the Cocos part to the west with a wedge-shaped gap open to the north. This slab tearing is synchronous with the differential movement between the two parts. The eastward movement of the Farallon part is expressed by its counter-clockwise rotation about the pole located infinitely far to the north, while the counter-clockwise rotation of the Cocos part pivots on the northwest corner of the sheet. With this pivoting the Cocos part of the slab decreases

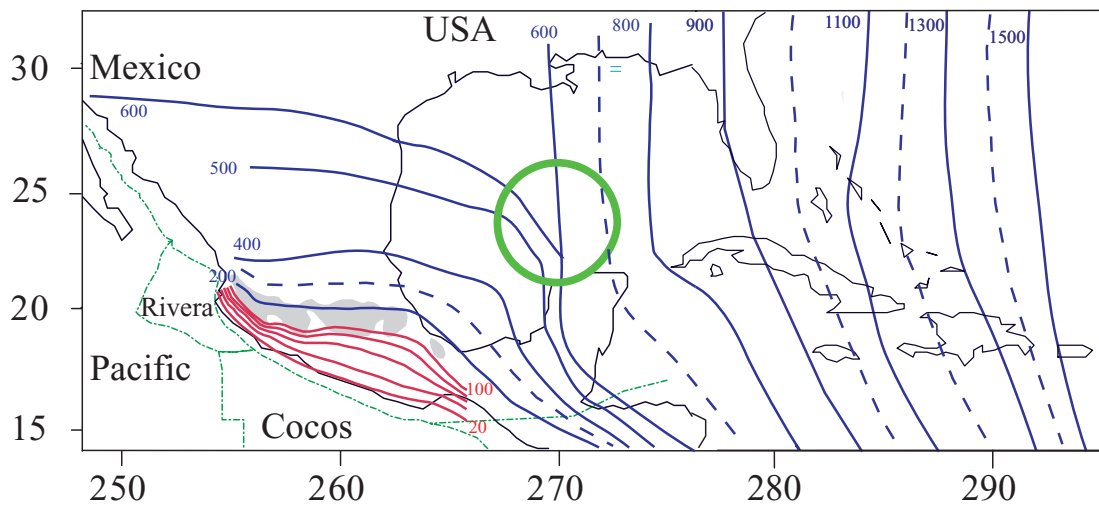


Figure 6. Configuration of the subducted plate superimposed on the tectonic map. Blue curves with numbers denote the upper surface of the subducted slab determined based on our tomographic model where numbers are depth in km. Deeper extension of the slab (deeper than 800 km) is refined using the tomographic model of Gorbatov *et al.* (2001). Blue dashed curves are interpolated isodepth values. The green circle shows the area where detachment of the Cocos slab from the Farallon slab might be occurring by slab tearing.

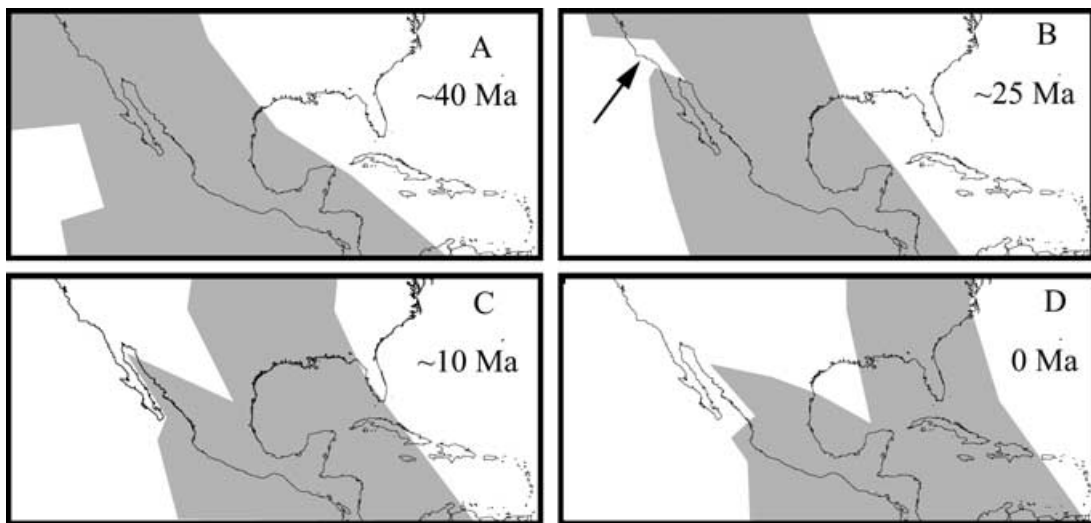


Figure 7. Sketch describing progressive development of the Farallon slab tear. The Farallon Plate is marked as a grey area. (a) About 40 Ma: the Farallon Plate before the start of mid-oceanic ridge subduction and plate segmentation. (b) About 25 Ma: initiation of mid-oceanic ridge subduction and development of the slab window (arrow). (c) About 10 Ma: progressive widening of the slab tear. (d) Present-day configuration of the plate involved in subduction.

its subduction rate rapidly to the north along the assumed north-south trending convergence boundary, while the subduction rate of the Farallon part remains uniform along it. This differential plate rotation geometrically induces relative uplift of the Cocos slab in its unbroken part. This relative uplift creates two slab scarps facing roughly north and east, as observed in our tomographic image. We suggest that the slab tearing is an ongoing process associated with the differential motion of the Cocos Plate and the already subducted slab of the Farallon Plate and is responsible for the distinctive configuration of the Wadati-Benioff zone and the east-west trending volcanic belt.

ACKNOWLEDGMENTS

We thank R. van der Hilst, P. Mann, and an anonymous referee for valuable suggestions which greatly improved the manuscript.

REFERENCES

- Barckhausen, U., Ranero, C.R., von Huene, R., Cande, S.C. & Roeser, H.A., 2001. Revised tectonic boundaries in the Cocos Plate off Costa Rica: implications for the segmentation of the convergent margin and for plate tectonic models, *J. geophys. Res.*, **106**, 19 207–19 220.
- DeMets, C., Gordon, R.G., Argus, D.F. & Stein, S., 1990. Current plate motions, *Geophys. J. Int.*, **101**, 425–478.
- Dickinson, W.R. & Snyder, W.S., 1979. Geometry of subducted slabs related to San Andreas Transform, *J. Geol.*, **87**, 609–627.
- Engdahl, E.R., van der Hilst, R.D. & Buland, R.P., 1998. Global teleseismic earthquake relocation from improved travel times and procedures for depth determination, *Bull. seism. Soc. Am.*, **88**, 722–743.
- Engebretson, D.C., Cox, A. & Gordon, R.G., 1985. Relative motions between oceanic and continental plates in the Pacific basin, *Geol. Soc. Am. Spec. Pap.*, **206**, 1–59.

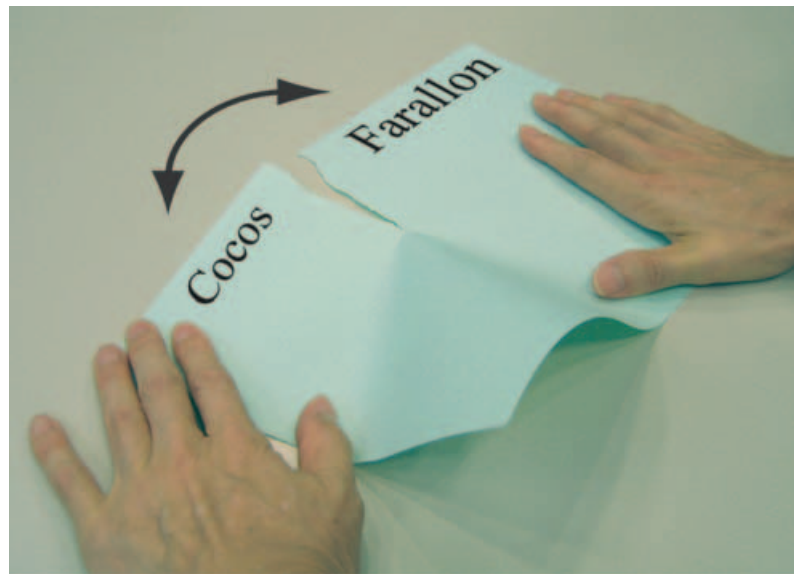


Figure 8. Schematic demonstration of the slab tearing process. The paper sheet represents the subducted slab, with the Farallon slab on the right and the Cocos slab on the left. The gap between these slabs is widening to the north, a process inherent in the differential rotation of the Cocos Plate relative to the Farallon Plate subduction. The slab tearing contorts the Cocos slab to elevate it.

- Ferrari, L., Lopez-Martinez, M., Aguirre-Diaz, G. & Carrasco-Nunez, G., 1999. Space-time patterns of Cenozoic arc volcanism in central Mexico: from the Sierra Madre Occidental to the Mexican Volcanic belt, *Geology*, **27**(4), 303–306.
- Fukao, Y., Widiyantoro, S. & Obayashi, M., 2001. Stagnant slabs in the upper and lower mantle transition region, *Rev. Geophys.*, **39**, 291–323.
- Grand, S.P., van der Hilst, R.D. & Widiyantoro, S., 1997. Global seismic tomography: a snapshot of convection in the Earth, *GSA Today*, **7**, 1–7.
- Gorbatov, A., Fukao, Y. & Widiyantoro, S., 2001. Application of a three-dimensional ray-tracing technique to global P, PP and Pdiff traveltime tomography, *Geophys. J. Int.*, **146**, 583–593.
- Kennett, B.L.N., Engdahl, E.R. & Buland, R., 1995. Constraints on seismic velocities in the earth from travel times, *Geophys. J. Int.*, **122**, 108–124.
- Koketsu, K. & Sekine, S., 1998. Pseudo-bending method for three-dimensional seismic ray tracing in a spherical earth with discontinuities, *Geophys. J. Int.*, **132**, 339–346.
- Lithgow-Bertelloni, C. & Richards, M.A., 1998. The dynamics of Cenozoic and Mesozoic plate motions, *Rev. Geophys.*, **36**, 27–78.
- Lonsdale, P., 1991. Structural patterns of the Pacific floor offshore of peninsular California, in *Gulf and Peninsula Province of the Californias*, American Association of Petroleum Geologists Memoir 47, pp. 87–125, eds Dauphin, J.P. & Simoneit, B.T., American Association of Petroleum Geologists, Tulsa, OK.
- Moran-Zenteno, D.J., Corona-Chavez, P. & Tolson, G., 1996. Uplift and subduction erosion in south-western Mexico since the Oligocene: pluton geobarometry constraints, *Earth planet. Sci. Lett.*, **141**, 51–65.
- Nicholson, C., Sorlien, C.C., Atwater, T., Crowell, J.C. & Luyendyk, B.P., 1994. Microplate capture, rotation of the western Transverse Ranges, and initiation of the San Andreas transform as a low-angle fault system, *Geology*, **22**, 491–495.
- Pardo, M. & Suarez, G., 1995. Shape of the subducted Rivera and Cocos plates in southern Mexico: seismic and tectonic implications, *J. geophys. Res.*, **100**, 12 357–12 373.
- Severinghaus, J. & Atwater, T., 1990. Cenozoic geometry and thermal state of the subducting slabs beneath western North America, in *Basin and Range Extensional Tectonics Near the Latitude of Las Vegas, Nevada*, Geological Society of America Memoir 176, pp. 1–22, ed. Wernicke, B.P., Geological Society of America, Boulder, CO.
- Stock, J. & Molnar, P., 1988. Uncertainties and implications of the Late Cretaceous and Tertiary position of North America relative to Farallon, Kula and Pacific plates, *Tectonics*, **7**, 1339–1384.
- Thorkelson, D.J., 1996. Subduction of diverging plates and the principles of slab window formation, *Tectonophysics*, **255**, 47–63.
- van der Hilst, R.D., 1990. Mantle structure below convergent margins, *PhD thesis*, Utrecht University, Utrecht, the Netherlands.
- van der Hilst, R.D., Widiyantoro, S. & Engdahl, E.R., 1997. Evidence for deep mantle circulation from global tomography, *Nature*, **386**, 578–584.
- van der Lee, S. & Nolet, G., 1997. Seismic image of the subducted trailing fragments of the Farallon plate, *Nature*, **386**, 266–269.
- Wortel, R. & Cloetingh, S., 1981. On the origin of the Cocos – Nazca spreading center, *Geology*, **9**, 425–430.